DOI 10.36146/2026_04_20

Construction of heat treatment analysis model considering transformation plasticity and accuracy verification

T. Fujisawa

In steel product manufacturing, the demand for thermo-mechanical controlled processing (TMCP) is rising to achieve various desired properties. However, uneven temperature distribution during cooling can cause shape defects. Therefore, accurately predicting thermal deformation is vital for optimizing cooling conditions. This task is challenging because thermal deformation results from complex interactions among strain, heat transfer, and phase transformations. In particular, transformation plasticity significantly influences final product quality, affecting shape and residual stresses. This study developed a thermal deformation prediction model that incorporates transformation plasticity through multi-phase transformations. The model's accuracy and validity were assessed by comparing experimental results with simulations of camber in plate samples subjected to one-sided spray cooling. The findings revealed discrepancies between experiments and simulations that excluded transformation plasticity, whereas including it led to good agreement. This prediction method enhances the understanding of TMCP processes.

KEYWORDS: HEAT TREATMENT; PHASE TRANSFORMATION; TRANSFORMATION PLASTICITY; TMCP; CAMBER; WATER COOLING; THERMAL DEFORMATION;

INTRODUCTION

In the manufacturing of steel products, the demand for thermo-mechanical controlled processing (TMCP) is steadily increasing to satisfy various property requirements. However, shape defects occur when the temperature distribution of steel products becomes uneven during the cooling process. As a result, productivity and product yield decrease. Predicting thermal deformation with high accuracy is essential for optimizing cooling conditions and improving productivity. However, it is difficult to predict thermal deformation after the cooling process because it is a complex phenomenon involving interactions among strain, heat transfer, and phase transformation [1, 2]. In particular, "transformation plasticity" is known to play an important role as it affects final product quality, such as shape and residual stresses. Previous studies have analyzed transformation plasticity considering single-phase transformations, such as bainitic and martensitic transformations [3, 4]. On the other hand, there are few analyses that consider transformation plasticity through multi-phase transformations.

In this study, a thermal deformation prediction model

Takuya Fujisawa
JFE Steel Corporation, Japan

considering transformation plasticity through multi-phase transformations was developed to achieve high accuracy. The accuracy and validity of the analysis were evaluated by comparing experimental and simulated camber results of SUS304 and S25C plate samples after one-sided spray cooling.

MATERIAL AND EXPERIMENTAL PROCEDURE

The materials used in the experiment were Japanese Industrial Standards (JIS) SUS304 and S25C steel. The former does not undergo phase transformation because it is a quasi-stable austenitic steel, whereas the latter does. Table 1 shows their chemical compositions, expressed in weight percentages.

Figure 1 shows a schematic illustration of the specimen. In the experiment, square specimens measuring 200 mm on each side and 20 mm thick were used, with four thermocouples inserted at representative positions to measure temperature history. Table 2 presents the water cooling conditions used in the experiment. The water flow density had varied to change the phase transformation and the amount of camber after cooling.

Figure 2 shows a schematic illustration of the experimental equipment. The specimen was heated to 1000°C in an electric furnace, then removed and fixed on a stand. After that, cooling water was sprayed from the spray nozzle with the shutter closed. When the specimen temperature, as indicated by the thermocouples, reached 900°C, the shutter was opened, and the specimen was cooled down to nearly 30°C. Cooling water was supplied by a pump from a reservoir tank maintained at 30°C. The water was sprayed onto the entire cooling surface through a spray nozzle mounted above the specimen, resulting in an approximately square spray area. The flow density was calculated by dividing the nozzle flow rate by the spray area. After cooling, the specimens were scanned in the widthwise direction using a laser displacement meter to evaluate the amount of camber.

Tab.1 - Chemical composition of materials. Reprinted and translated from T. Fujisawa [5] with permission of the Iron and Steel Institute of Japan. Copyright (2024) the Iron and Steel Institute of Japan.

	C	Si	Mn	P	S	Cu	Ni	Cr
SUS304	0.04	0.56	0.91	0.035	0.002	-	8.09	18.18
S25C	0.23	0.17	0.37	0.02	0.018	0.12	0.05	0.12

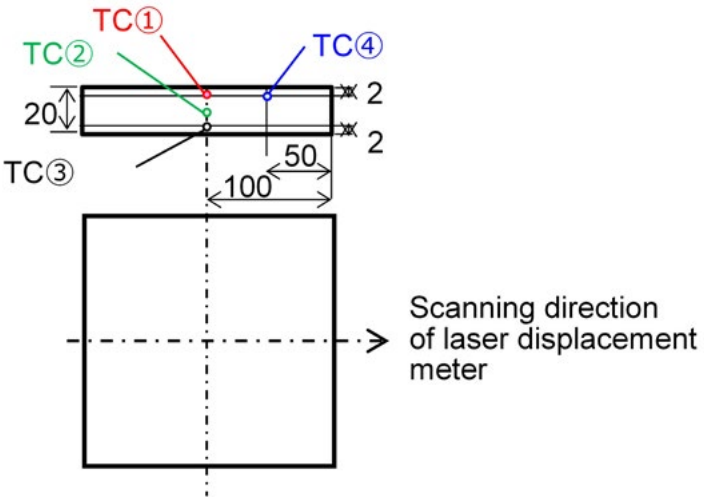

Fig.1 - Schematic illustration of specimen. Reprinted and translated from T. Fujisawa [5] with permission of the Iron and Steel Institute of Japan. Copyright (2024) the Iron and Steel Institute of Japan.

Tab.2 - Water cooling condition. Reprinted and translated from T. Fujisawa [5] with permission of the Iron and Steel Institute of Japan. Copyright (2024) the Iron and Steel Institute of Japan.

	Mild cooling	Intensive cooling
Nozzle model number	3/8KS0555SQ	3/8KS1760Q
Injection distance [mm]	300	190
Flow rate [L/min]	3	17
Flow density [L/m^{2}min]	30	407

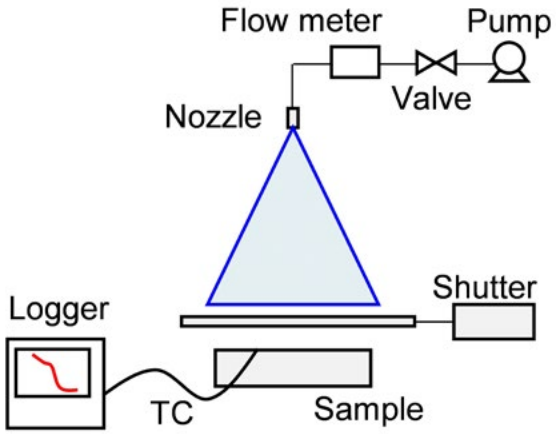

Fig.2 -Schematic illustration of experimental equipment. Reprinted and translated from T. Fujisawa [5] with permission of the Iron and Steel Institute of Japan. Copyright (2024) the Iron and Steel Institute of Japan.

FINITE ELEMENT MODELING

In this study, the analysis software ABAQUS Standard 2018 was used. The following contents were implemented as subroutines to develop a prediction model capable of performing coupled analyses of phase transformation, temperature, and strain. Phase fractions were calculated using a method based on the TTT diagram for arbitrary temperature histories [6]. The start of phase transformation into ferrite and pearlite, which are diffusional transformations, as well as bainite, which is intermediate between diffusional and diffusionless transformations, is expressed by equation 1. The phase transformation begins when the incubation period consumption I reaches I = 1. Here, I is the incubation period, T is current temperature, t is time, and the subscript s represents the start of phase transformation in the TTT diagram.

$$I = \int \frac{dt}{t_s(T)} \qquad [1]$$

The JMAK-type isothermal transformation rate equation was used to calculate the progress of phase transformation [7], where f represents the transformation fraction, and n and k are constants. The subscripts F,P,B and eq denote ferrite, pearlite, bainite, and the equilibrium transformation rate, respectively.

$$f_{F,P,B} = f_{eq}\{1 - exp(-kt^n)\} \qquad [2]$$

The initiation and progression of martensite, a diffusionless transformation, were governed by the modified Koistinen-Marburger law [8] and implemented in the user subroutine UFIELD. Material properties, including the TTT diagram, were obtained using the material performance simulation software JMatPro. Mechanical and thermal properties were defined by considering the temperature dependence of each individual phase and were determined from the transformation ratios of each phase using the linear mixing rule.

The total strain increment was expressed by equation 3 to account for transformation plastic strain, which represents the interaction between strain and phase transformation. Here, the subscripts e,p,th,m and TP denote elastic strain, plastic strain, transformation expansion, transformation strain, and transformation plastic strain, respectively.

$$d\varepsilon = d\varepsilon_e + d\varepsilon_p + d\varepsilon_{th} + d\varepsilon_m + d\varepsilon_{TP} \qquad [3]$$

In particular, for transformation plastic strain in the case of multi-phase transformation, equation 4 was used based on the reports by Yanagisawa et al. [4] and Taleb et al. [9]. Here, K is the transformation plasticity coefficient, σ_d is the deviatoric stress, the subscript j represents each phase except austenite, and the subscript γ denotes austenite. These definitions were implemented in the user subroutine UEXPAN.

$$d\varepsilon_{TP} = \sum_j 3K_j\{f_\gamma df_j\}\sigma_d \qquad [4]$$

MODEL GEOMETRY AND FE MESH

Figure 3 shows the model geometry, finite element FE mesh, and boundary conditions. To simulate the experiment in which one side of the plate was water-cooled, a cross-sectional half model was constructed by considering symmetry at the center of the width. The model consisted of a total of 2,000 elements and 2,121 nodes. The element size was 1.0 × 1.0 mm. Thermal boundary conditions were imposed on the top surface, defined by the following equation:

$$q = h(T_s - T_w) \qquad [5]$$

where q is the heat flux, h is the heat transfer coefficient, T_s is the current temperature, and T_w is the water temperature, set at 30°C. The heat transfer coefficient was determined from experimental temperature history. Figure 4 shows an example of the heat transfer coefficient under intensive cooling conditions.

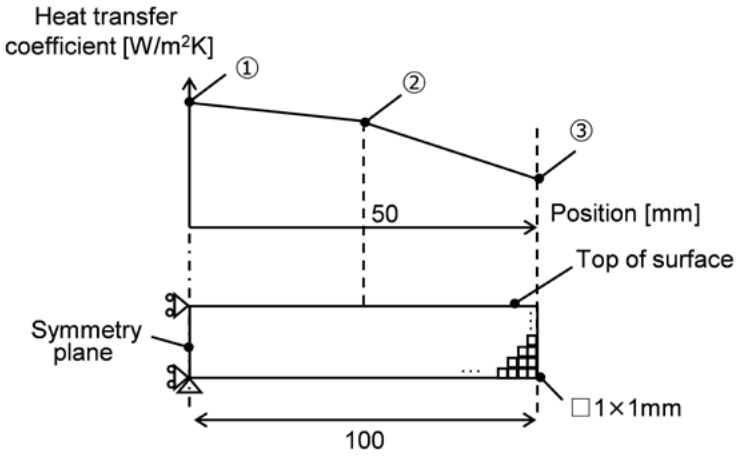

Fig.3 - Model geometry, FE mesh and boundary condition. Reprinted and translated from T. Fujisawa [5] with permission of the Iron and Steel Institute of Japan. Copyright (2024) the Iron and Steel Institute of Japan.

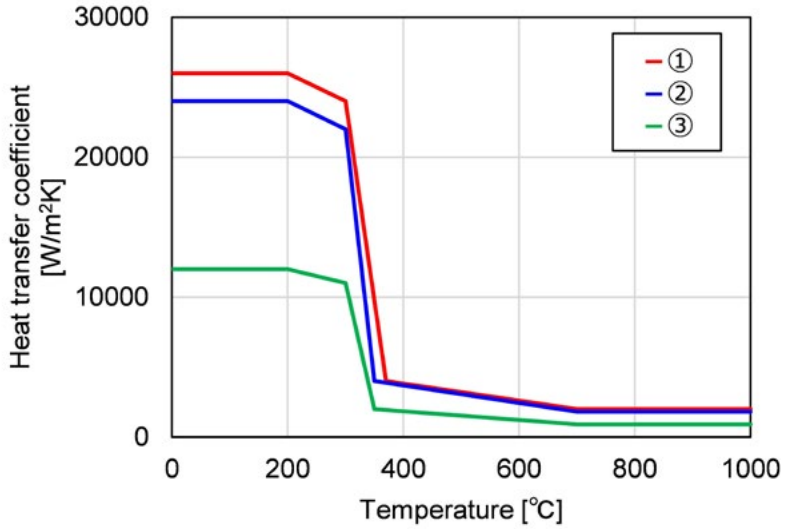

Fig.4 - Heat transfer coefficient (intensive cooling). Reprinted and translated from T. Fujisawa [5] with permission of the Iron and Steel Institute of Japan. Copyright (2024) the Iron and Steel Institute of Japan.

EXPERIMENTAL AND ANALYSIS RESULT

Figure 5 shows experimental and analytical thermal history of S25C under intensive cooling conditions as an example. It could be confirmed that the thermal history of analysis result was in accordance with that of experimental result. The obtained thermal history was similar to the typical thermal history observed when using boiling refrigerants such as water. In the initial stage of cooling, the temperature dropped slowly due to film boiling, thereafter, the temperature transitioned to nucleate boiling state and dropped rapidly. A similar thermal history was observed for SUS304, and it was confirmed that the experiment and analysis were consistent. Figure 6 shows analytical results for temperature distribution of S25C under intensive cooling at representative times. As can be seen in figure 6, the temperature on the top of surface was lower during water cooling, indicating uneven cooling.

Figure 7 shows analytical results for the phase fraction distribution of S25C after cooling under intensive cooling as an example. The calculation results showed that the top of surface had approximately 90% bainite and the bottom of surface had approximately 90% ferrite and pearlite and 10% bainite, resulting in an overall transformation to three phases. On the other hand, in the case of mild cooling conditions, the proportion of ferrite in the cross section was high, at about 50 to 80%. And the remaining 20 to 50% was transformed into pearlite, resulting in an overall transformation to two phases. From the above calculation results, it was estimated that the microstructure after cooling differs due to difference in cooling conditions even in the experiment. Note that SUS304 does not undergo phase transformation, so it remained austenite before and after cooling regardless of the cooling conditions.

As an example, figure 8 shows the experimental and analytical results for the camber of SUS304 and S25C after cooling under intensive cooling. For SUS304, since no phase transformation occurs, transformation plasticity was not considered. However, the amount of and direction of camber tended to be consistent.

On the other hand, in the case of S25C occurring phase transformation, when not considering transformation plasticity (as indicated in figure 8, without TP), the amount of camber after cooling did not match between the experiment and analysis.

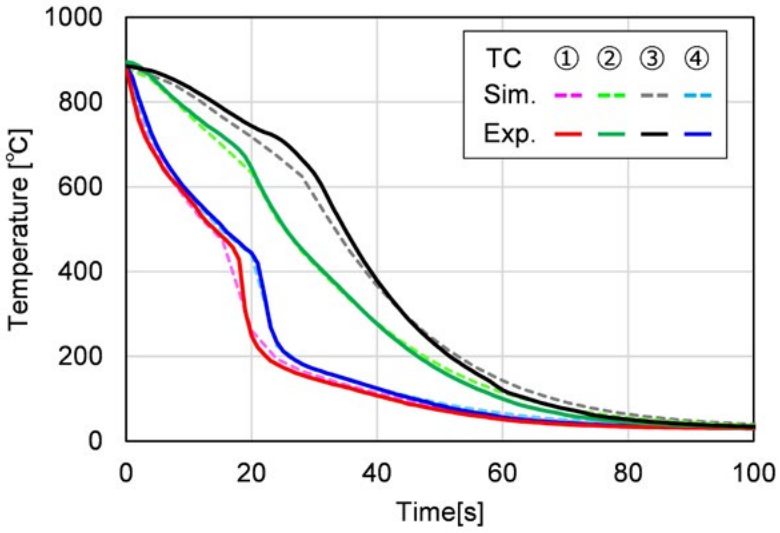

Fig.5 - Experimental and analytical thermal history of S25C (intensive cooling). Reprinted and translated from T. Fujisawa [5] with permission of the Iron and Steel Institute of Japan. Copyright (2024) the Iron and Steel Institute of Japan.

However, when considering transformation plasticity (as indicated in figure 8 with TP), the amount of camber tended to be more consistent with the experiment. It can be stated that considering transformation plasticity is important for accurately predicting the thermal deformation associated with phase transformation.

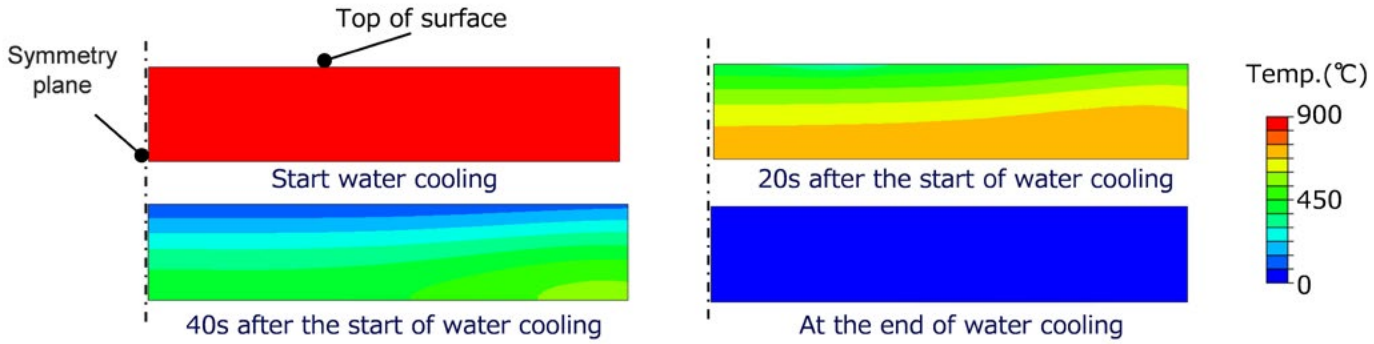

Fig.6 - Analytical results for temperature distribution S25C after cooling under intensive cooling.

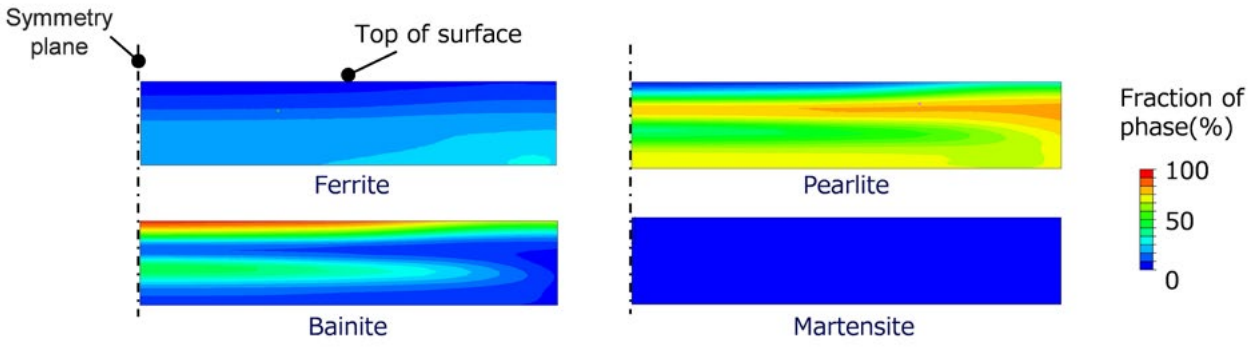

Fig.7 - Analytical results for the phase fraction of S25C after cooling under intensive cooling.

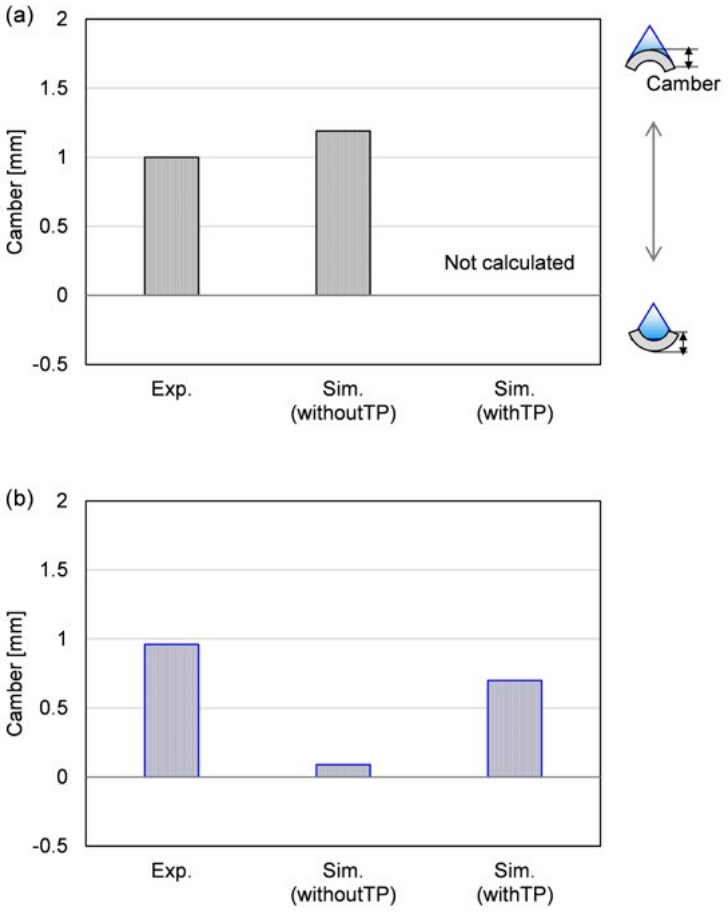

Fig.8 - Comparison of experimental and analysis camber after cooling (intensive cooling): (a) SUS304, (b) S25C. Reprinted and translated from T. Fujisawa [5] with permission of the Iron and Steel Institute of Japan. Copyright (2024) the Iron and Steel Institute of Japan.

CONCLUSIONS

In this study, a thermal deformation prediction model considering transformation-induced plasticity through multi-phase transformation was developed with high accuracy. The accuracy and validity of the analysis were evaluated by comparing experimental and simulated camber of SUS304 and S25C plate samples after one-sided spray cooling. As a result, when phase transformation occurs during heat treatment, neglecting transformation plasticity in the analysis leads to deviations in the predicted camber compared to experimental results. Conversely, incorporating transformation plasticity improves the agreement between predicted and experimental camber, enhancing prediction accuracy. In other words, it was confirmed that accounting for transformation plasticity is essential for accurately predicting thermal deformation. Furthermore, since the predicted camber generally agreed well with experimental data, this analysis method is considered valid even when multi-phase transformations occur. The thermal deformation prediction method that includes transformation plasticity contributes to a deeper understanding of TMCP.

In addition, this paper including above figures (1~5, 8) and tables (1, 2) is reprinted and translated from T. Fujisawa [5] with permission of the Iron and Steel Institute of Japan. Copyright (2024) the Iron and Steel Institute of Japan.

REFERENCES

[1] T. Inoue, T. Yamaguchi, Z. Wang, "Stresses and phase transformations occurring in quenching of carburized steel gear wheel," Materials Science and Technology, 1985, vol. 1, pp. 872-876. https://doi.org/10.1179/mst.1985.1.10.872

[2] S. Denis, S. Sjöström, A. Simon, "Coupled temperature, stress, phase transformation calculation model numerical illustration of the internal stresses evolution during cooling of a eutectoid carbon steel cylinder," Metallurgical Transactions A, 1987, vol. 18, pp. 1203-1212. https://doi.org/10.1007/BF02647190

[3] S. Yamanaka, T. Sakanoue, T. Yoshii, T. Inoue, "Influence of transformation plasticity on the distortion of carburized quenching process of Cr-Mo steel ring," Journal of the Society of Materials Science, 1999, vol. 48, pp. 733-739. https://doi.org/10.2472/jsms.48.733

[4] Y. Yanagishawa, T. Hosoya, M. Minamiya, K. Saitoh, "Modeling simulation of transformation plasticity in a multi-phase transformation," Nihon Seiko Technical report, 2019, vol. 70, pp. 32-38. https://doi.org/10.1016/j.ijmecsci.2018.08.025

[5] T. Fujisawa, "Construction of heat treatment analysis model considering transformation plasticity and accuracy verification," CAMP-ISIJ, 2024, vol. 37, No. 2, pp. 350-353 (in Japanese).

[6] E. Scheil, "Anlaufzeit der Austenitumwandlung," Archiv fur das Eisenhuttenwesen, 1935, vol. 12, pp. 565-567. https://doi.org/10.1002/srin.193500186

[7] M. Umemoto, I. Tamura, "Continuous cooling transformation kinetics of steels," Tetsu-to-Hagane, 1982, vol. 68, pp. 383-392. https://doi.org/10.2355/tetsutohagane1955.68.3_383

[8] D. P. Koistinen, R. E. Marburger, "A general equation prescribing the extent of the austenite-martensite transformation in pure iron-carbon alloys and plain carbon steels," Acta Metallurgica, 1959, vol. 7, pp. 59-60. https://doi.org/10.1016/0001-6160(59)90170-1

[9] L. Taleb, S. Petit, "New investigations on transformation induced plasticity and its interaction with classical plasticity," International Journal of Plasticity, 2006, vol. 22, pp. 110-130. https://doi.org/10.1016/j.ijplas.2005.03.012

TORNA ALL'INDICE >